01 Jan 2005

Performance of a BGO PET/CT with Higher Resolution PET Detectors

John W. Wilson
Missouri University of Science and Technology, jwilson@mst.edu

Timothy G. Turkington

J. J. Williams

James G. Colsher

et. al. For a complete list of authors, see https://scholarsmine.mst.edu/min_nuceng_facwork/1192

Recommended Citation

J. W. Wilson et al., "Performance of a BGO PET/CT with Higher Resolution PET Detectors," *IEEE Nuclear Science Symposium Conference Record, 2005*, Institute of Electrical and Electronics Engineers (IEEE), Jan 2005.
The definitive version is available at https://doi.org/10.1109/NSSMIC.2005.1596701

Performance of a BGO PET/CT with Higher Resolution PET Detectors

Timothy G. Turkington, *Member, IEEE*, John J. Williams, *Senior Member, IEEE,* John W. Wilson, James G. Colsher, *Member, IEEE*, David L. McDaniel, Chang L. Kim, Steve G. Ross, *Member, IEEE,* Charles W. Stearns, *Senior Member, IEEE*, Scott D. Wollenweber, *Member, IEEE*

***Abstract*–A new PET detector block has been designed to replace the standard detector of the Discovery ST PET/CT system. The new detector block is the same size as the original, but consists of an 8x6 (tangential x axial) matrix of crystals rather than the original 6x6. The new crystal dimensions are 4.7 x 6.3 x 30 mm3 (tangential x axial x radial). Full PET/CT systems have been built with these detectors (Discovery STE). Most other aspects of the system are identical to the standard Discovery ST, with differences including the low energy threshold for 3D imaging (now 425 keV) and front-end electronics. Initial performance evaluation has been done, including NEMA NU2-2001 tests and imaging of the 3D Hoffman brain phantom and a neck phantom with small lesions. The system sensitivity was 1.90 counts/s/kBq in 2D, and 9.35counts/s/kBq in 3D. Scatter fractions measured for 2D and 3D, respectively, were 18.6% and 34.5%. In 2D, the peak NEC of 89.9 kcps occurred at 47.0 kBq/cc. In 3D, the peak NEC of 74.3 kcps occurred at 8.5 kBq/cc. Spatial resolution (all expressed in mm FWHM) measured in 2D for 1 cm off-axis source 5.06 transaxial, 5.14 axial and for 10 cm source 5.45 radial, 5.86 tangential, and 6.23 axial. In 3D for 1cm off-axis source 5.13 transaxial, 5.74 axial, and for 10 cm source 5.92 radial, 5.54 tangential, and 6.16 axial. Images of the brain and neck phantom demonstrate some improvement, compared to measurements on a standard Discovery ST.**

I. Introduction

A new detector block has been developed for the Discovery ST PET/CT (GE Healthcare Technologies, Milwaukee, WI) [1]. This block has the same overall dimensions of the original block but is segmented into more, smaller crystals. The original block was a 6x6 matrix of 6.3 mm x 6.3 mm x 30 mm BGO crystals. The newer block is an 8x6 matrix of 4.7 mm x 6.3 mm x 30 mm BGO crystals, The crystal arrays are shown in Fig. 1. This design was expected to yield higher transverse spatial resolution while retaining the count sensitivity and count rate performance of the original.

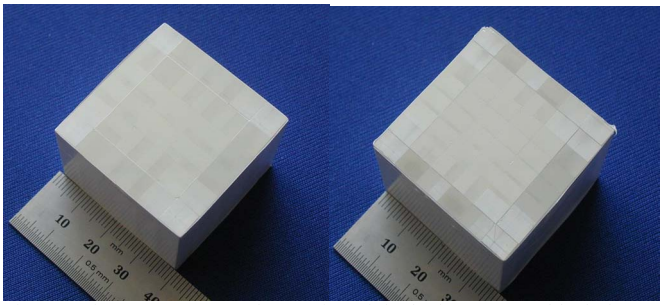

Fig. 1 Left: 6x6 BGO crystal array for original Discovery ST block detector. Right: 8x6 Crystal array for Discvory STE block detector. The reduced crystal size is in the transverse direction.

PET/CT systems have been built with the new PET detector module (Discovery STE, GE Healthcare Technologies, Milwaukee, WI). In addition to the block/crystal differences, these new systems operate with a low energy threshold of 425 keV, compared to 375 keV for the Discovery ST. Previous measurements on a Discovery ST indicated that the trade-off between lower sensitivity and improved scatter fraction is overall improved, based on count statistics, for a variety of object sizes, with the higher threshold [2]. In addition, a new front-end data acquisition scheme has been implemented.

We have performed a series of measurements to evaluate the PET performance of the Discovery STE, including basic NEMA NU2-2001 measures and image quality comparisons with the Discovery ST for phantoms with realistic but relatively high count density phantoms, for which the improvements in intrinsic spatial resolution were expected to have the biggest gain.

II. Methods

System sensitivity, scatter fraction, count rate performance, and spatial resolution were all measured according to the NEMA NU2-2001 specifications [3].

Imaging studies were performed with two phantoms, both of which represent relatively high-count-density imaging situations. Discovery ST imaging was performed at Duke University Medical Center, while the Discovery STE imaging was performed at the GE Healthcare Technologies factory.

A. Hoffman 3D Brain Phantom

The Hoffman 3D Brain Phantom was scanned on both systems filled with 1 mCi of F-18 solution. The phantom was positioned so that the slices within the phantom would match as well as possible by using the CT scout image to set the PET field of view (FOV) to start at the top of the phantom for the

Manuscript received November 11, 2005. This work was supported in part by the GE Healthcare Technologies, Milwaukee, WI.

T. G. Turkington is with the Dept. of Radiology of Duke University Medical Center, Durham, NC 27710 USA (telephone: 919-684-7706, e-mail: timothy.Turkington@duke.edu).

J. W. Wilson is with the Dept. of Radiology of Duke University Medical Center, Durham, NC 27710, U.S.A

J. J. Williams is with GE Healthcare Technologies, Milwaukee, WI (e-mail: john.j.williams@med.ge.com)

J. G. Colsher, D. L. McDaniel, C. L. Kim, S. G. Ross, C. W. Stearns, and S. D. Wollenweber are also with GE Healthcare Technologies, Milwaukee, WI

studies on both systems. Imaging was done in 3D mode, and lasted 6 min. Images were reconstructed with the 3D reprojection method, and corrections including CT-based attenuation correction, model-based scatter correction, and singles-based randoms correction. Images were reconstructed with a 25.6 cm transverse FOV, into a 128x128x47 matrix. For the Discovery ST, images were reconstructed with the ramp filter only. For the Discovery STE, images were reconstructed three ways: ramp only, and two levels of moderate smoothing. The highest level of smoothing was a modified Hann filter that, based on line source data, provided the same reconstructed resolution as ramp-filtered Discovery ST data.

B. Neck Phantom

A neck phantom has been developed in the Duke University Medical Center PET Facility to evaluate specific protocols for imaging head and neck cancer patients. The current protocol includes a long (8 min) scan of the most superior field of view in the whole-body exam, which descends ~15 cm from the base of the brain, and includes the primary regions of interest for head and neck cancers. In addition to the long scan, some of the head and neck area has relatively low attenuation for the emitted photons (especially compared to thorax and abdomen), independently resulting in higher count densities than obtained elsewhere. The resulting data are reconstructed with a finer pixels (~2 mm) than are typically used for whole body imaging, with the assumption that higher-count images could allow the detection and characterization of smaller lesions.

Fig. 2. The neck phantom.

The phantom is a 11.5 cm diameter, 12.5 cm tall cylinder with 8 internal small fillable spheres. There were two spheres of each of the following internal diameters: 4.4 mm, 6.0 mm, 7.7 mm, and 9.8 mm. All were positioned at a radius of 3 cm in an octagonal pattern, with the the 4.4 mm and 9.8 mm spheres in one plane and the 6.0 and 7.7 mm spheres in another. The phantom is shown in Fig. 2. This phantom was filled with 7.4 kBq/cc F-18 solution in the background, and 8x that concentration in the spheres, measured volumetrically. An 8 min 2D scan was performed, again using the CT scout image to align the phantom similarly in the two systems.

Images were reconstructed with filtered back-projection and with OS-EM, using a 256x256 image matrix covering a 50 cm field of view, using CT-based attenuation correction, scatter correction, and singles-based randoms correction. Filtered back-projection images were reconstructed with a ramp filter only for the DST data (cut-off of 6.3 mm), and DST were reconstructed two ways

III. Results

A. System Sensitivity

The average (over r=0 and r=10 cm) sensitivity for the DSTE was 1.90 (2D) and 9.35 (3D) cps/kBq, compared to reported values [1] of 1.95 (2D) and 9.2 (3D) for the DST.

B. Scatter Fraction

Scatter fractions were 18.6% (2D) and 34.5% (3D) for the DSTE, compared to reported values of 19% (2D) and 45% (3D) for the DST.

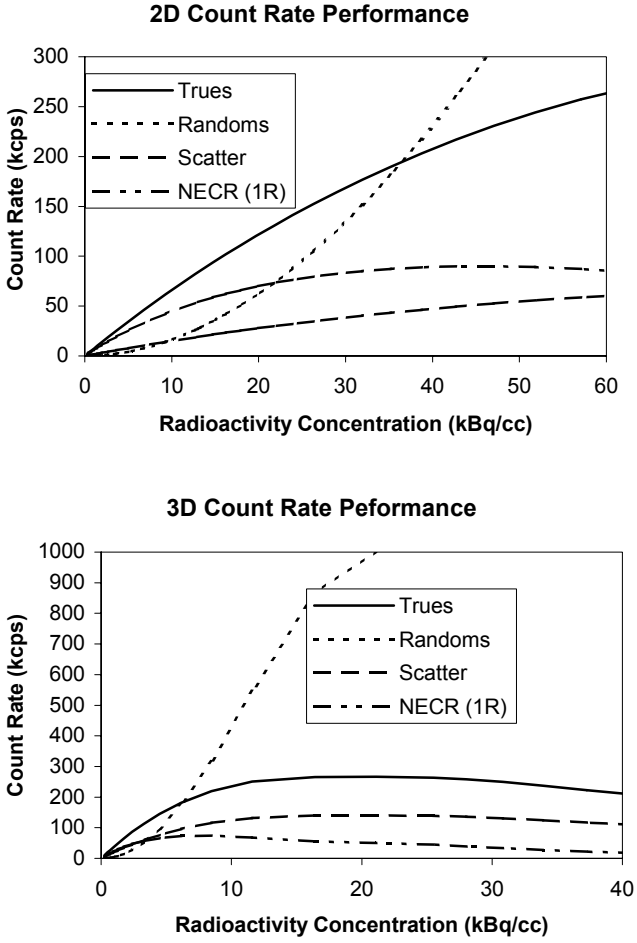

Fig. 3. NEMA NU2-2001 Count rate performance in 2D and 3D modes.

C. Count Rate Performance

Count rate performance in 2D and 3D is shown in Fig. 3. Peak NECR in 2D is 89.9 kcps at a radioactivity concentration of 47.0 kBq/cc in 3D is 74.3 kcps at a radioactivity concentration of 8.5 kBq/cc.

D. Spatial Resolution

Measured spatial resolution results are shown in Table I. All values are full-width at half-maximum (FWHM). Improvements are seen in the transverse measurements, compared to the Discovery ST values, with r=1 cm values now approximately 5 mm.

TABLE I
INTRINSIC SPATIAL RESOLUTION

All values FHWM, measured in mm

	DSTE		DST	
	2D	3D	2D	3D
1 cm off-axis				
transaxial	5.06	5.13	6.13	6.11
axial	5.14	5.74	5.18	5.97
10 cm off-axis				
radial	5.45	5.92	6.72	6.77
tangential	5.86	5.54	6.99	6.78
axial	6.23	6.16	6.12	6.69

E. Hoffman Brain Phantom

Images from the 3D Hoffman brain phantom are shown in Fig. 4. Two slices of the phantom are shown from the Discovery ST image set and the three Discovery STE image sets. Many of the brain structures are similarly visualized on all image sets. A few of the cortical features are better delineated on the DSTE images. Whereas the DST produces acceptable images without any smoothing, the ramp filter alone on the DSTE yielded somewhat noisy images. This is due to the higher Nyquist frequency for the better sampling.

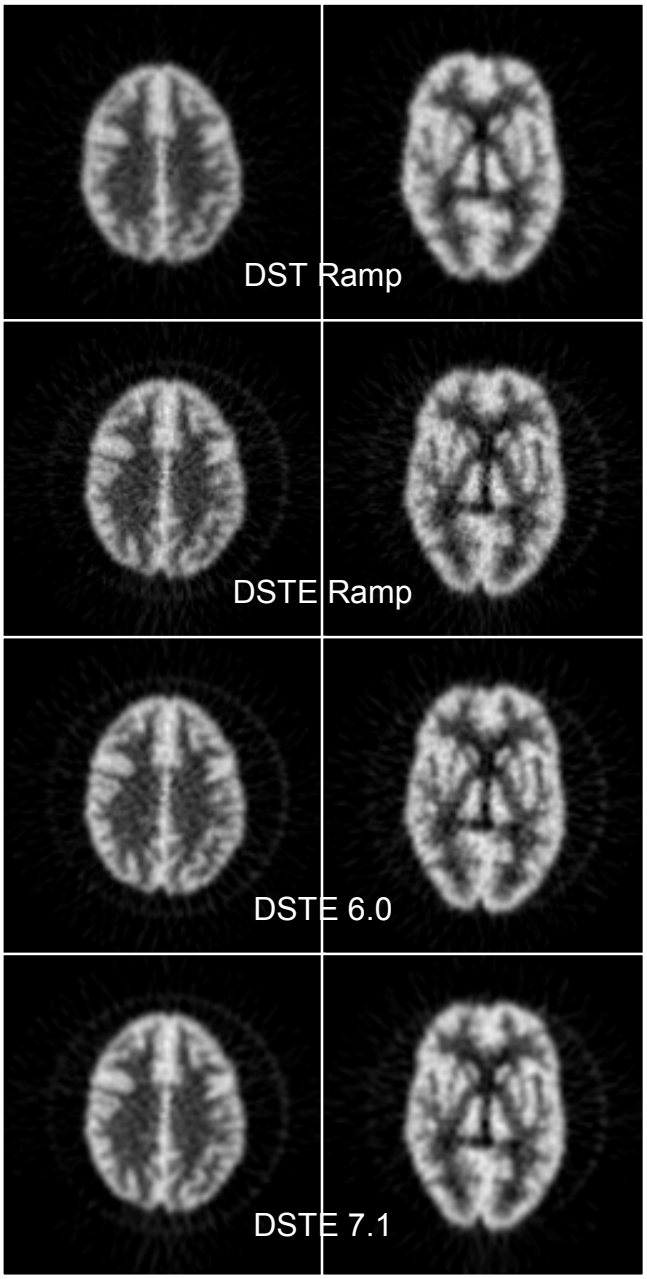

Fig. 4. 3D Hoffman Brain Phantom images. At top are images from the Discovery ST. The three lower rows are DSTE images, witn 6.0 and 7.1 representing the degree of smoothing. 7.1 provides similar spatial resolution to ramp-filtered DST images.

F. Neck Phantom

Images from the neck phantom are shown in Fig. 5. These images were reconstructed with two iterations of OS-EM, with 21 (DST) and 20 (DSTE) subsets. The slice shown includes on of the smallest spheres (4.4 mm) and both of the large spheres (0.98 mm). Profiles are shown to depict the small sphere. The intensity of a small sphere depends on a variety of factors, including how well the sphere is centered in the slice, and this could not be controlled precisely between the studies on the two scanners. Nevertheless, the small spheres were consistently more conspicuous in the DSTE images than in the DST.

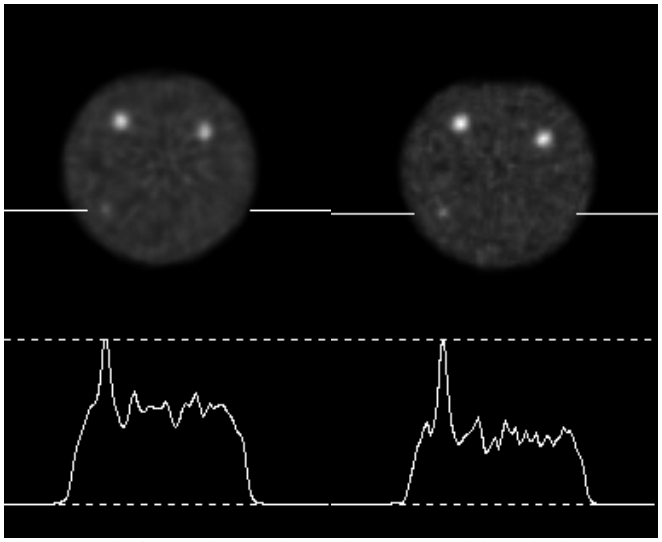

Fig. 5. Neck phantom images from Discovery ST (left) and Discovery STE (right) showing the 1 cm spheres and 1of the 4.4 mm spheres. The profile is placed on the 4.4 mm sphere.

A more quantitative indicator of the improved image quality was obtained by drawing a circular ROI on each sphere in each image set and recording the maximum pixel. Each result was divided by the mean from a large background ROI on the same slice. These values were measured for the OS-EM images and for filtered back-projection images reconstructed with several filters. The results were averaged for the two spheres of each size class. For the DST, ramp only was used (with cut-off in spatial domain of 6.3 mm). For the DSTE, ramp only (with a cut-off in spatial domain of 4.8 mm), and then the modified Hann which yields the same line source resolution as ramp on the DST (referred to as 7.1). The results are shown in Fig. 6 for the 6, 8, and 10 mm sphere pairs.

In all cases, the contrast is better for the DSTE images than for the DST (comparing the ramp-filtered FBP with FBP, OSEM with OSEM). The DSTE 7.1 values are more similar to the DST values, as expected, since they were smoothed so as to match the resolution. The differences in contrast (between DST and DSTE) are greater for the smaller spheres than for the 10 mm spheres, as may be expected since spatial resolution differences would be most important for the smallest object.

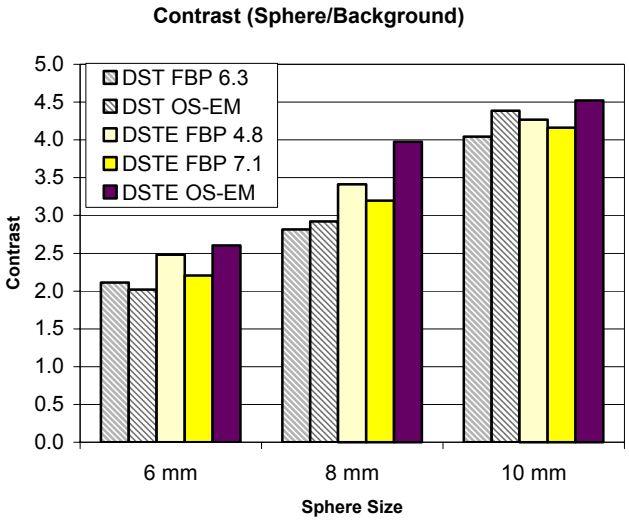

Fig. 6. Contrast measurement of hot spheres in neck phantom. The dashed bars are DST measures, and solid are DSTE.

IV. Discussion and Conclusions

Smaller crystal elements were expected to yield improved spatial resolution, and indeed that was the case. The resolution did not following the reduction in crystal size proportionately, with FWHM resolution slightly better than the crystal size for the larger crystal, and slight worse than the crystal size for the smaller crystals.

Count rate and scatter fraction improvements are attributable to the new 425 keV energy threshold.

Image quality has improved for the high-count-density studies performed. Whether the improved intrinsic spatial resolution will benefit more typical whole-body imaging situations is not as clear, and will be more difficult to evaluate.

Acknowledgment

We thank Dr. Yuka Yamamoto for discussion regarding the head and neck cancer application.

References

[1] O. Mawlawi, D. A. Podoloff, S. Kohlmyer, J.J. Williams, C.W. Stearns, R.F. Culp, H. Macapinlac, "Performance Characteristics of a Newly Developed PET/CT Scanner using NEMA Standards in 2D and 3D Modes," *J Nucl Med* vol. 45, no. 10, pp. 1734-1742, 2004.

[2] T.G. Turkington, J. W. Wilson, and J. G. Colsher, "Adjusting the Low Energy Threshold for Large Bodies in PET," in *Proceedings of 2004 IEEE Nuclear Science Symposium and Medical Imaging Conference*.

[3] National Electrical Manufacturers Association. NEMA Standards Publication NU-2 2001, "Performance Measurements of Positron Emission Tomographs," Rosslyn, VA: National Electrical Manufacturers Association; 2001.